Journal of
Materials Chemistry C

Materials for optical, magnetic and electronic devices

Accepted Manuscript

This article can be cited before page numbers have been issued, to do this please use: J. Kang, G. Park, D. Han, S. Kim, M. Jung, K. Kim, I. Oh, H. Oh and K. Son, *J. Mater. Chem. C*, 2026, DOI: 10.1039/D6TC00615A.

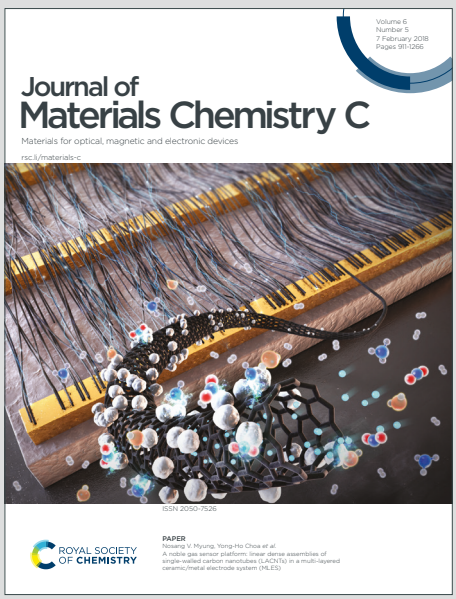

ROYAL SOCIETY OF CHEMISTRY

rsc.li/materials-c

View Article Online
DOI: 10.1039/D6TC00615A

ARTICLE

Composition-Dependent Magnetic Anisotropy in Cu/Mn-Based Two-Dimensional Hybrid Perovskite Single Crystals

Received 00th January 20xx,
Accepted 00th January 20xx

DOI: 10.1039/x0xx00000x

Jiho Kang,[‡a] Garam Park,[‡a] Dongyoung Han,[a] Sunghyun Kim,[b] Minji Jung,[b] Ki-Yeon Kim,[c] In Hwan Oh,[c] Hyunchul Oh*[b], Kwanghyo Son*[a]

We report the composition-dependent magnetic anisotropy of two-dimensional Ruddlesden-Popper hybrid perovskite single crystals, $(C_6H_5CH_2CH_2NH_3)_2CuCl_4$ (Cu-PEA), $(C_6H_5CH_2CH_2NH_3)_2MnCl_4$ (Mn-PEA), and mixed Cu/Mn compositions. All samples crystallize in a layered structure (Pbca) characteristic of two-dimensional hybrid halide perovskites. X-ray diffraction confirms that the mixed crystals preserve the same structural motif while exhibiting systematic lattice variations with composition. Magnetic measurements reveal distinct ground states for the end members: Cu-PEA shows ferromagnetic ordering with a Curie temperature of 12 K, whereas the Mn-PEA exhibits antiferromagnetic behavior with a Néel temperature of 44 K, while a broader magnetic feature around 80 K reflects short-range magnetic correlations. The mixed Cu/Mn crystals display a composition-dependent evolution of magnetization magnitude and magnetic anisotropy, reflecting the interplay between Cu-based ferromagnetic and Mn-based antiferromagnetic interactions within the layered structure. Curie–Weiss analysis and two-dimensional Heisenberg modeling further indicate direction-dependent exchange interactions, highlighting the intrinsic anisotropic spin coupling of the layered framework. These results demonstrate that compositional mixing provides an effective route to tuning magnetic anisotropy while maintaining the crystallographic structure.

Introduction

The wide chemical versatility of organic cations, metal cations, and halide anions offers abundant opportunities to tailor the physical and chemical properties of hybrid materials for diverse applications. Among these systems, organic–inorganic halide materials—including metal–organic frameworks[1-4] and metal-organic crystals,[5-8] have attracted sustained interest owing to their remarkable electrical, thermal, and optical properties. In particular, organic–inorganic halide perovskites (OIHPs) have emerged as highly promising materials, especially in the field of photovoltaics.[9-11] Their distinctive structural flexibility and tunable electronic characteristics have established them as leading candidates for semiconductor devices, most notably high-efficiency solar cells.[12-15]

OIHP materials combine the complementary advantages of both organic and inorganic components.[16, 17] The organic constituents enable structural flexibility and facile solution processability, allowing the formation of diverse layered and composite frameworks. In contrast, the inorganic metal–halide networks provide structural robustness under elevated temperatures and pressures and introduce a wide range of functional properties, including magnetism[18, 19] and electrical conductivity.[20, 21] Owing to this synergistic combination, OIHPs have become highly attractive platforms for both fundamental studies and emerging applications across physics, chemistry, and materials science.

OIHPs have demonstrated outstanding performance as light-absorbing materials, with significant advances in light absorption, charge transport, defect tolerance, and luminescence stability.[22-25] Their efficient separation of photoexcited carriers has led to remarkable improvements in the power conversion efficiency of perovskite solar cells.[26] Despite these achievements, investigations into their magnetic properties remain comparatively limited, as most studies have primarily focused on electrical, thermal, and optical functionalities. While three-dimensional perovskite structures have been extensively explored, their structural stability is often compromised under humid conditions, prolonged light exposure, and elevated temperatures.[27] In contrast, two-dimensional perovskites, particularly those adopting a Ruddlesden–Popper (RP) configuration, exhibit enhanced environmental stability owing to their layered architecture. In the RP structure, metal–halide octahedra form two-dimensional sheets separated by organic spacer layers, with hydrogen bonding between halide ions and ammonium groups reinforcing interlayer cohesion.[28] Such a layered framework provides a unique platform for tuning magnetic interactions through compositional modification of the metal sites or organic spacers. Consequently, RP-type OIHPs have emerged as promising candidates for magnetic switches, quantum devices, spintronic systems, and nanoscale magnetic semiconductors.[29-32] A deeper understanding of their intrinsic magnetic behavior

[a] Department of Physics Education, Kongju National University, Gongju 32588, Republic of Korea
[b] Department of Chemistry, UNIST, Ulsan 44919, Republic of Korea
[c] Neutron Science Division, Korea Atomic Energy Research Institute, Daejeon 34057, Republic of Korea

† Electronic supplementary information (ESI) available. See DOI:

View Article Online
DOI: 10.1039/D6TC00464A

is therefore essential for advancing their functional applications.

Recent studies have demonstrated that introducing a second transition metal cation into 2D hybrid perovskites at low dopant concentrations (x<0.1) can modify magnetic parameters such as the Néel temperature and suppress spin-flop transitions without altering the overall magnetic ground state of the host.[33] However, the evolution of magnetic anisotropy across the full composition range spanning from one magnetic ground state to another and its quantitative, direction-resolved characterization remain largely unexplored. In this study, we investigate the magnetic properties of two-dimensional Ruddlesden–Popper hybrid perovskite single crystals, $(C_6H_5CH_2CH_2NH_3)_2ACl_4$ (*A*-PEA, A = Cu, Mn), together with compositionally mixed Cu/Mn analogues, $(C_6H_5CH_2CH_2NH_3)_2Cu_xMn_{1-x}Cl_4$ (Cu_xMn_{1-x}-PEA, x=0.25, 0.5, 0.75). The end-member compounds exhibit distinct magnetic ground states, with Cu-PEA showing ferromagnetic ordering and Mn-PEA displaying antiferromagnetic behavior. Mixed Cu/Mn single crystals were synthesized via a solution-based evaporation method, and their structural and magnetic properties were systematically characterized using X-ray diffraction (XRD) and vibrating sample magnetometry (VSM). Our results reveal that compositional mixing within the same layered crystallographic framework leads to a composition-dependent evolution of magnetization and magnetic anisotropy. Unlike previous studies focused on the low-doping regime, the present work explores the full composition range using single crystals to provide direction-resolved quantification of exchange interactions, offering insight into how competing Cu-centered ferromagnetic and Mn-centered antiferromagnetic interactions govern the evolution of magnetic anisotropy in layered hybrid perovskites.

Results and discussion

Description of Structures

As illustrated in Figure 1, the X-ray diffraction (XRD) patterns of the single-crystal samples, including Cu-PEA, Mn-PEA, and Cu_xMn_{1-x}-PEA(x=0.75, 0.5, 0.25), are shown. The Cu/Mn mixed crystals were grown from precursor solutions containing both Cu^{2+} and Mn^{2+} ions in the desired stoichiometric ratios under identical solution-evaporation conditions. Rietveld refinement of the room-temperature data confirms that both Cu-PEA and Mn-PEA crystallize in an orthorhombic layered structure (*Pbca*, No.61), with lattice parameters a = 7.198 Å, b = 7.375 Å, c = 38.550 Å fir Cu-PEA (Figure S1 a)), and a = 7.207 Å, b = 7.301 Å, c = 39.413 Å for Mn-PEA (Figure S1 b)). These values are consistent with previous reports.[34, 35] The crystallite sizes of Cu-PEA and Mn-PEA were estimated from the Scherrer equation using the (0 0 4) reflextion, yielding values of 34.4 nm and 35.2 nm, respectively (Tables S1), consistent with the high crystallinity of the single-crystal samples. For the mixed Cu_xMn_{1-x}-PEA compositions, independent Rietveld refinement was not feasible due to the coexistence of Cu- and Mn-rich domains. However, the diffraction peak positions of the mixed samples coincide with those of the end-members, confirming that the same crystallographic framework (Pbca) is preserved across all compositions. Composition-dependent peak shifts

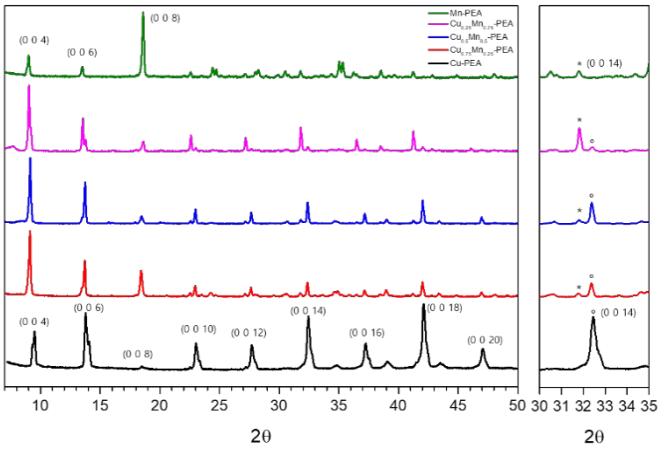

Figure 1. X-ray diffraction (XRD) patterns of single-crystal $(C_6H_5CH_2CH_2NH_3)_2ACl_4$ (*A* = Cu, Mn) and mixed Cu_xMn_{1-x}-PEA (x = 0.75, 0.50, 0.25) samples. All compositions adopt an layered structure (Pbca). Composition-dependent peak shifts and partial splitting are observed in the mixed samples, reflecting lattice parameter modulation associated with Cu/Mn compositional variation within the same crystallographic framework.

accompanied by slight broadening and partial splitting are observed at selected reflections, attributed to local lattice parameter modulation arising from the intrinsic difference in ionic radii between Cu^{2+} and Mn^{2+}. No additional well-defined secondary phases are detected within the instrumental resolution. Representative single-crystal images are provided in Figure S2. Within the instrumental resolution, the absence of additional impurity reflections suggests that the structural evolution arises from compositional modulation within a common crystallographic framework rather than from macroscopic phase segregation.

The observed variations in peak positions can be attributed to differences in ionic radii between Cu^{2+} and Mn^{2+} within the layered perovskite framework. This effect becomes more pronounced in the Cu/Mn mixed compositions (Cu_xMn_{1-x}-PEA), where composition-dependent peak shifts accompanied by

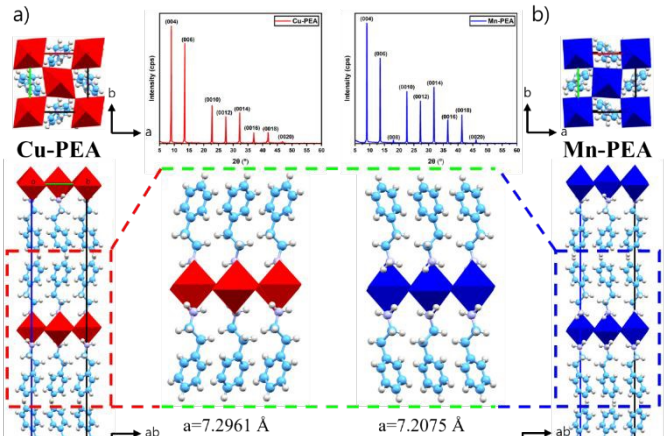

Figure 2. Structural characterization of single-crystal a) Cu-PEA and b) Mn-PEA. XRD patterns reproduced from Ref. 36 are shown alongside the corresponding crystal structure models for structural confirmation. Both compounds adopt an Ruddlesden–Popper structure (Pbca), consisting of two-dimensional metal–halide octahedral layers separated by phenethylammonium spacer layers. The structural models highlight the layered stacking along the c-axis and the arrangement of the inorganic framework within the plane.

View Article Online
DOI: 10.1039/D6TC00615A

partial splitting are observed at selected reflections. These features reflect lattice parameter modulation arising from Cu/Mn compositional variation within the same orthorhombic structure. The diffraction patterns indicate that the mixed crystals preserve the overall crystallographic framework of the end members while accommodating local structural distortions associated with compositional changes. An image of the fabricated single crystal is shown in Figure S3.

Crystallographic analysis

The XRD patterns and corresponding crystal structure models of Cu-PEA and Mn-PEA are presented in Figure 2[36], confirming the Ruddlesden–Popper framework (Pbca). X-ray diffraction (XRD) analysis confirms that all samples share closely related diffraction features, indicating a common crystallographic framework. Miller index analysis verifies that both Cu-PEA and Mn-PEA crystallize in the same space group (Pbca). The diffraction patterns are dominated by reflections along the c-axis, consistent with the highly anisotropic layered nature of the two-dimensional Ruddlesden–Popper structure. The significantly larger lattice parameter along the c-axis compared to the a- and b-axes further reflects the extended stacking of inorganic metal–halide sheets separated by organic spacer layers. Comparison of the indexed reflections with previous studies confirms that the crystal structure of Cu-PEA agrees well with the report by Polyakov et al.[37], while Mn-PEA is consistent with the structure reported by Park et al.[38]. Both compounds adopt a two-dimensional Ruddlesden–Popper perovskite framework. Although the overall structural motif is preserved, slight differences in lattice parameters arise from the different ionic radii and electronic configurations of Cu^{2+} and Mn^{2+} within the metal–halide layers, leading to subtle variations in layer spacing and octahedral distortion.

Temperature-dependent magnetization curve (M-T curve)

The temperature-dependent magnetization (M–T) curves of the five single-crystal samples are shown in Figure 3. All measurements were performed under an applied magnetic field of 1000 Oe in both in-plane and out-of-plane configurations. Cu-PEA exhibits ferromagnetic ordering in both orientations, with a Curie temperature (T_C) of approximately 12 K, as determined from the derivative of the M–T curves. A clear enhancement of magnetization is observed below T_C in both geometries, indicating robust spin alignment within the layered framework. In the out-of-plane configuration, a subtle anomaly appears near 6.2 K, where the magnetization shows a slight increase followed by a reduction at lower temperatures, suggesting anisotropic spin behavior associated with the two-dimensional structure. In contrast, Mn-PEA displays predominantly antiferromagnetic behavior with a Néel temperature of approximately 80 K in both orientations. The magnetization decreases below T_N, consistent with antiferromagnetic ordering. The in-plane data show a non-monotonic temperature dependence at low temperatures, which may reflect anisotropic spin interactions or slight spin canting within the layered structure rather than long-range ferromagnetic ordering. For the Cu_xMn_{1-x}-PEA samplesthe overall magnetization magnitude evolves systematically with composition, decreasing as the Mn fraction increases. A low-temperature magnetic transition is observed near 12 K in all

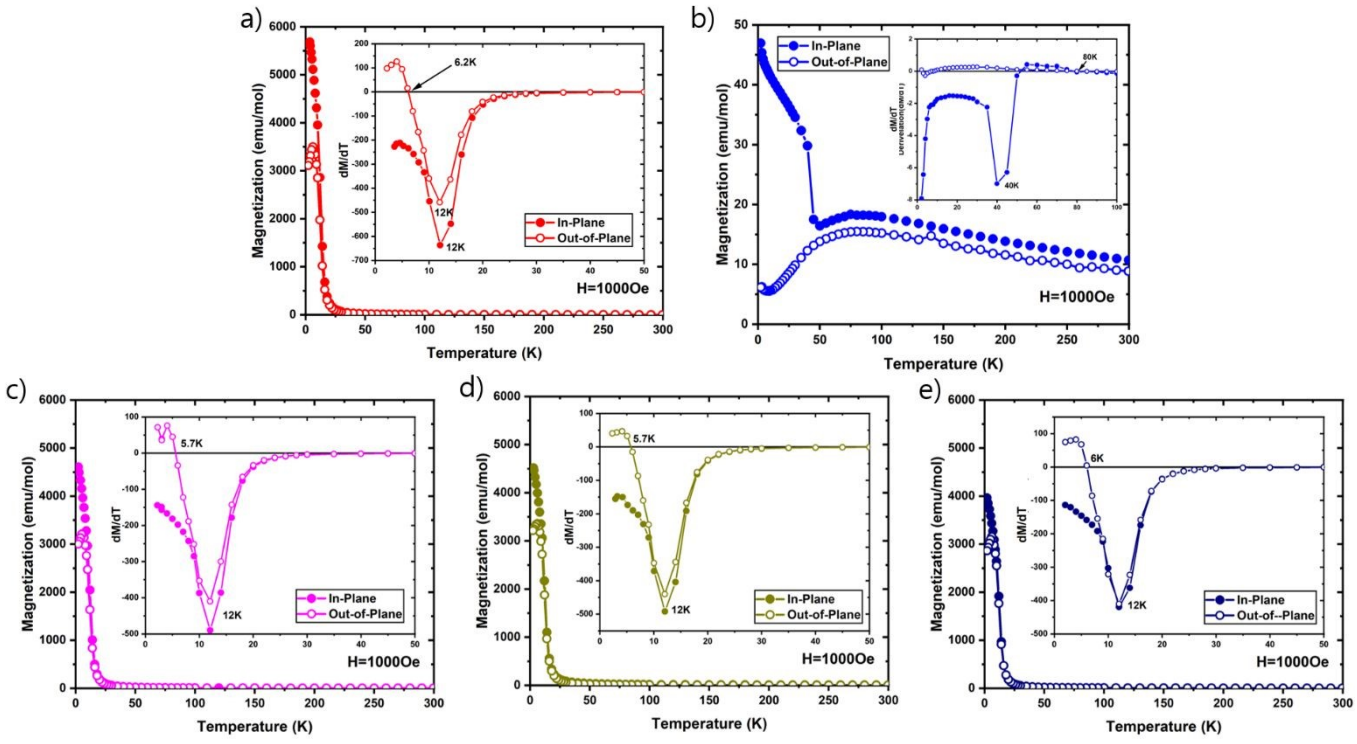

Figure 3. Temperature-dependent magnetization (M–T) measured under an applied field of 1000 Oe for a) Cu-PEA, b) $Cu_{0.75}Mn_{0.25}$-PEA, c) $Cu_{0.50}Mn_{0.50}$-PEA, d) $Cu_{0.25}Mn_{0.75}$-PEA, and e) Mn-PEA single crystals in both in-plane and out-of-plane configurations. Cu-PEA exhibits ferromagnetic ordering near 12 K, whereas Mn-PEA shows antiferromagnetic behavior with a transition near 80 K. The mixed compositions display composition-dependent evolution of low-temperature magnetic features within the same layered framework.

View Article Online
DOI: 10.1039/D6TC00615A

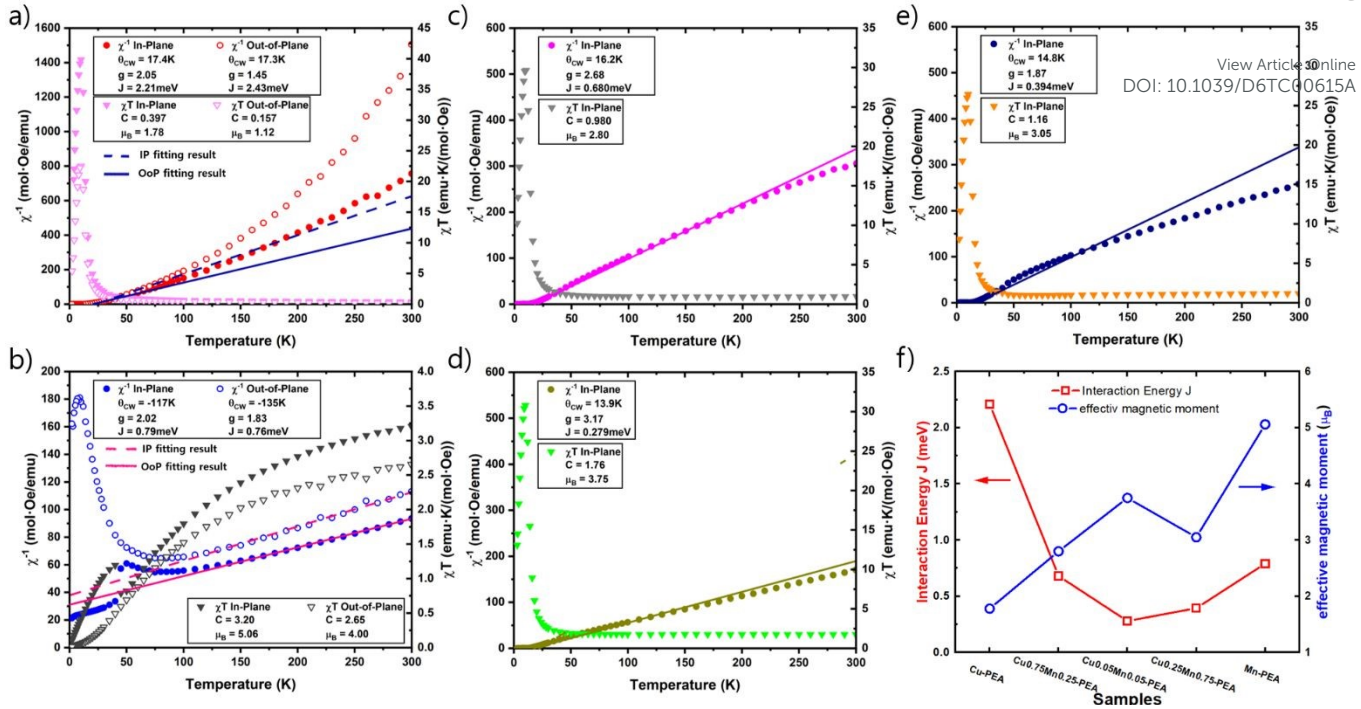

Figure 4. Temperature dependence of inverse magnetic susceptibility (χ^{-1}) and χT for a) Cu-PEA, b) Mn-PEA, c) $Cu_{0.75}Mn_{0.25}$-PEA, d) $Cu_{0.50}Mn_{0.50}$-PEA, and e) $Cu_{0.25}Mn_{0.75}$-PEA measured in the in-plane configuration. Solid lines represent fits to the Curie–Weiss law and two-dimensional Heisenberg model. The Weiss temperature (θ_{CW}), Landé g-factor (*g*), exchange interaction energy (*J*), Curie constant (*C*), and effective magnetic moment (μ_{eff}) were extracted from the fitting analysis. F) Composition-dependent evolution of the exchange interaction energy (J, red) and effective magnetic moment (μ_{eff}, blue) as a function of sample composition, summarizing the systematic variation magnetic parameters across the Cu/Mn series.

mixed compositions, consistent with the characteristic ordering temperature of Cu-PEA. The persistence of this feature suggests that Cu-related ferromagnetic interactions remain influential within the layered framework across the composition range. In addition, a secondary anomaly is observed near 5–6 K, whose prominence varies with composition. This behavior likely reflects the increasing contribution of Mn-related antiferromagnetic interactions and the resulting competition between Cu- and Mn-centered spin exchange pathways. This trend is further supported by the magnetic characterization of an additional composition, $Cu_{0.17}Mn_{0.83}$-PEA (Figure S3), which similarly exhibits a low-temperature transition near 12K alongside a negative Weiss temperature and a spin-flop-like feature in the M-H curve, consistent with the growing dominance of Mn-centered antiferromagnetic interactions at higher Mn content. The progressive decrease in magnetization amplitude and the composition-dependent evolution of a secondary anomaly near 5-6K whose prominence increases with Mn content indicate that the magnetic response in the mixed crystals arises from the interplay of Cu-centered ferromagnetic and Mn-centered antiferromagnetic exchange interactions within a common crystallographic structure, rather than from a simple superposition of independent phases. Notably, the primary ordering temperature near 12K remains essentially unchanged across all Cu-containing compositions, suggesting that Cu-related ferromagnetic interactions continue to govern the low-temperature ordering while Mn-centered interactions progressively modify the magnetic anisotropy and low-temperature behaviour. The magnetic susceptibility data were further analysed using the Curie-Weiss law and a two-dimensional Heisenberg model, as summarized in Figure 4 and Table1. The composition-dependent evolution of the exchange interaction energy (*J*) and effective magnetic moment (μ_{eff}) is presented in Figure 4f. The temperature dependence of the inverse susceptibility (χ^{-1}) was fitted to the Curie–Weiss relation, $\chi(T) = C/(T-\theta)$, where *C* is the Curie constant and θ is the Weiss temperature. To gain further insight into the exchange interactions within the layered framework, the susceptibility data were also fitted using analytical expressions derived for two-dimensional Heisenberg systems. The models employed for Cu-PEA and Mn-PEA were adopted from the formulations reported by Losee et al.[39] and Lines et al.[40], respectively. The corresponding expressions are given by:

For Cu-PEA:

$$\frac{1}{\chi} = \frac{4kT}{Ng^2\mu_B^2}\left[1 + 2\left(\frac{J}{kT}\right) + 2\left(\frac{J}{kT}\right)^2 + \frac{4}{3}\left(\frac{J}{kT}\right)^3 + \ldots\right]^{-1} \quad (1)$$

For Mn-PEA:

$$\frac{1}{\chi} = \frac{kT}{Ng^2\mu_B^2}\left[\begin{matrix}0.343 + 4\left(\frac{J}{kT}\right) + 12.7\left(\frac{J}{kT}\right)^2 + 17.5\left(\frac{J}{kT}\right)^3 \\ +176\left(\frac{J}{kT}\right)^4 + 680\left(\frac{J}{kT}\right)^5 + 872\left(\frac{J}{kT}\right)^6\end{matrix}\right] \quad (2)$$

Here, *N* denotes the number of spins, *g* is the Landé g-factor, μ_B is the Bohr magneton, and *J* represents the exchange interaction energy.

For Cu-PEA, the Curie–Weiss temperatures (θ_{CW}) were determined to be 17.4 K for the in-plane configuration and 17.3 K for the out-of-plane configuration. The positive θ_{CW} values in both orientations indicate the predominance of ferromagnetic exchange interactions above the ordering temperature. The

View Article Online
DOI: 10.1039/D6TC00615A

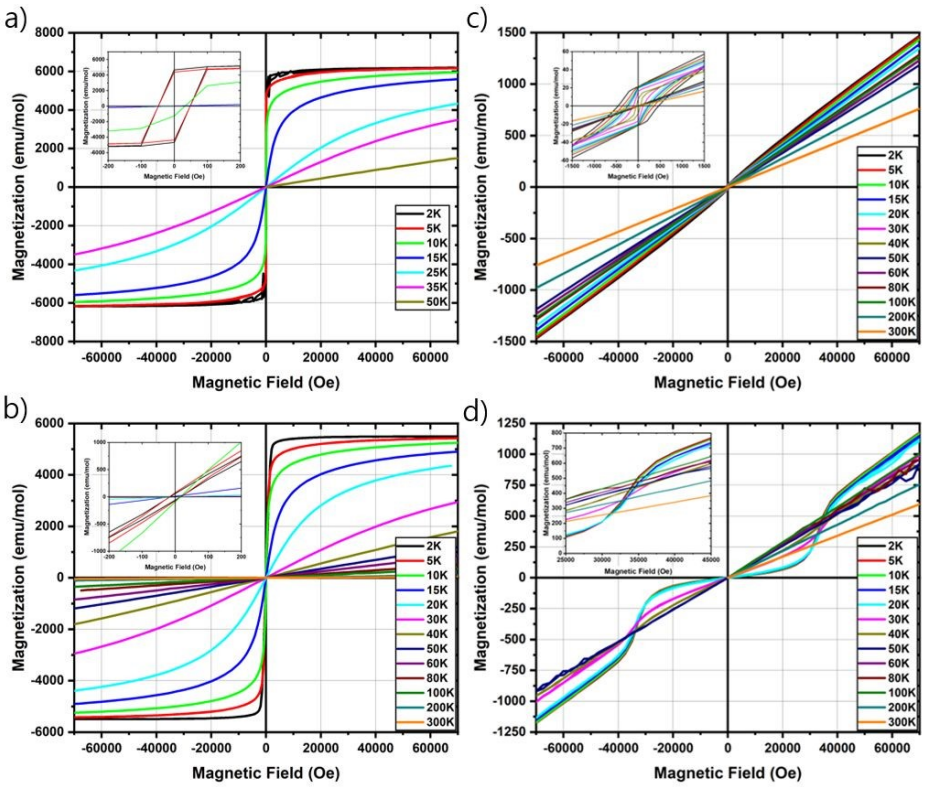

Figure 5.Magnetic field-dependent magnetization (M–H) curves measured at various temperatures for Cu-PEA and Mn-PEA single crystals. a) Cu-PEA (in-plane), b) Cu-PEA (out-of-plane), c) Mn-PEA (in-plane), and d) Mn-PEA (out-of-plane). The data illustrate the temperature evolution of magnetic hysteresis and anisotropic magnetic responses in the layered Ruddlesden–Popper framework.

Curie constants were obtained as 0.397 emu·K·mol^{-1} (in-plane) and 0.157 emu·K·mol^{-1} (out-of-plane). The theoretical effective magnetic moment for Cu^{2+} (S = 1/2) is 1.73 μ_B. Experimentally, the in-plane effective magnetic moment (1.78 μ_B) agrees well with this value, while the out-of-plane value (1.12 μ_B) is substantially reduced. This anisotropic reduction suggests direction-dependent spin susceptibility associated with the layered crystal structure, where magnetic interactions are primarily confined within the inorganic sheets. The extracted Landé g-factors are 2.05 (in-plane) and 1.45 (out-of-plane), indicating pronounced magnetic anisotropy. The exchange interaction energies, estimated from the two-dimensional Heisenberg model, are 2.21 meV (in-plane) and 2.43 meV (out-of-plane). Although the magnitudes are comparable, the directional dependence of g and μ_eff highlights anisotropic spin coupling intrinsic to the layered framework.

For Mn-PEA, the Curie–Weiss temperatures (θ_{CW}) were determined to be −117 K (in-plane) and −135 K (out-of-plane). The negative θ_{CW} values indicate dominant antiferromagnetic exchange interactions in both orientations. The Curie constants were obtained as 3.20 emu·K·mol^{-1} (in-plane) and 2.65 emu·K·mol^{-1} (out-of-plane). The theoretical effective magnetic moment for high-spin Mn^{2+} (d^5, S = 5/2) is 5.92 μ_B. Experimentally, the effective magnetic moments were 5.06 μ_B (in-plane) and 4.60 μ_B (out-of-plane), both slightly lower than the theoretical value. This reduction may arise from short-range antiferromagnetic correlations persisting above the Néel temperature, as well as anisotropic spin interactions within the layered structure. Compared to Cu-PEA, Mn-PEA exhibits a smaller net magnetization but a larger effective magnetic moment, reflecting the different electronic configurations of Mn^{2+} (d^5) and Cu^{2+} (d^9). While Mn^{2+} possesses a greater number of unpaired spins, the antiferromagnetic alignment of neighboring moments leads to partial cancellation of the macroscopic magnetization. The anisotropic values of μ_{eff} and θ_{CW} further suggest direction-dependent exchange interactions intrinsic to the two-dimensional Ruddlesden–Popper framework.

The Landé g-factors of Mn-PEA were determined to be 2.02 (in-plane) and 1.83 (out-of-plane), indicating moderate magnetic anisotropy within the layered structure. Although the anisotropy is less pronounced than in Cu-PEA, the directional difference in g suggests that spin responses are influenced by the two-dimensional crystal symmetry. The exchange interaction energies extracted from the two-dimensional Heisenberg model are 0.79 meV (in-plane) and 0.76 meV (out-of-plane), indicating comparable exchange strengths in both orientations. Despite the negative Weiss temperatures characteristic of antiferromagnetic interactions, the fitted exchange parameters reflect the magnitude of nearest-neighbor spin coupling within the model framework and do not directly imply ferromagnetic ordering. The small difference between in-plane and out-of-plane *J* values suggests that the exchange interactions are relatively isotropic in magnitude, while the observed anisotropy in μ_{eff} and g-factor highlights direction-dependent spin susceptibility inherent to the layered

View Article Online
DOI: 10.1039/D6TC00615A

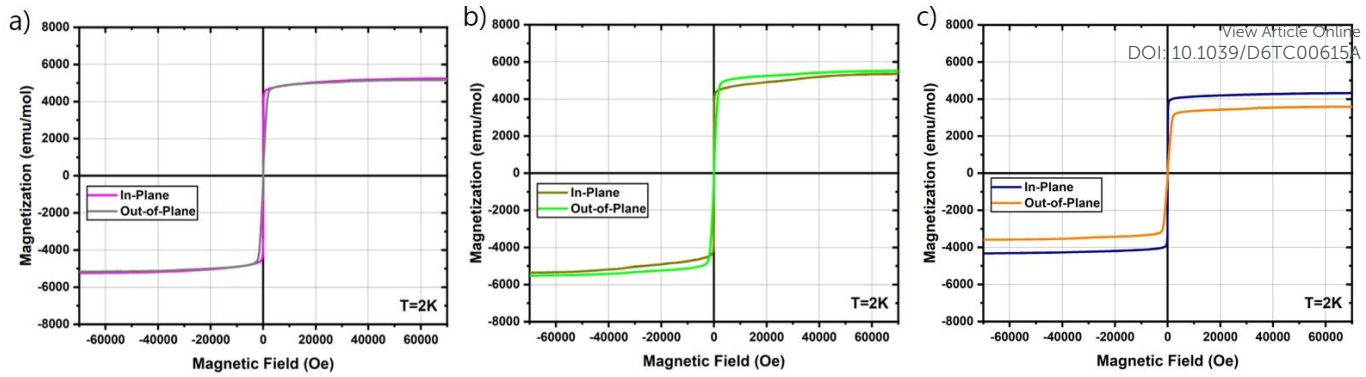

Figure 6. Magnetic field-dependent magnetization (M–H) curves measured at 2 K for a) $Cu_{0.75}Mn_{0.25}$-PEA, b) $Cu_{0.50}Mn_{0.50}$-PEA, and c) $Cu_{0.25}Mn_{0.75}$-PEA single crystals in both in-plane and out-of-plane configurations. The data illustrate the composition-dependent evolution of magnetic hysteresis and anisotropic magnetic response within the layered framework.

Ruddlesden–Popper structure. These results emphasize that the magnetic behavior of Mn-PEA arises from anisotropic exchange interactions governed by its two-dimensional structural framework. The magnetic susceptibility of the Cu_xMn_{1-x}-PEA samples was analyzed along the in-plane direction, corresponding to the magnetic easy axis. All mixed compositions exhibit positive Curie–Weiss temperatures, comparable in magnitude to that of Cu-PEA, indicating that ferromagnetic exchange interactions remain significant at low temperatures. However, the positive Weiss temperature does not necessarily imply long-range ferromagnetic ordering but rather reflects the dominance of Cu-related exchange interactions within the mixed system. The extracted Curie constants and effective magnetic moments fall between those of the Cu-PEA and Mn-PEA end members, consistent with compositional modulation of the spin population. The Landé g-factors remain anisotropic and comparable in magnitude to those of the parent compounds, suggesting that the layered crystal symmetry continues to govern the spin response. Although the exchange interaction energies (*J*) for the mixed samples are positive, their magnitudes are substantially reduced compared to Cu-PEA. This reduction indicates weakened coherent spin coupling, likely arising from compositional disorder and competing Cu- and Mn-centered exchange pathways within the same crystallographic framework. As summarized in Table 1 and Figure 4f, the exchange interation energy (J) decreases progressively with increasing Mn content, while the effective magnetic moment (μ_{eff}) increases, consistent with the growing contribution of Mn-centered antiferromagnetic interactions within the layered framework. Overall, the gradual evolution of θ_{CW}, μ_{eff}, and *J* with composition demonstrates tunable magnetic interactions governed by the interplay of distinct spin exchange mechanisms rather than by a simple superposition of independent magnetic phases.

Field-dependent magnetization curve (M-H curve)

Figures 5 and 6 present the magnetic field dependence of magnetization (M–H curves) for the single-crystal samples. The Cu-PEA and Mn-PEA end members were measured over a range of temperatures to examine the evolution of their magnetic behavior. In contrast, the Cu_xMn_{1-x}-PEA samples were characterized at 2 K to directly compare their low-temperature magnetic responses with those of the parent compounds. The low-temperature measurements of the mixed compositions enable evaluation of how Cu- and Mn-centered exchange interactions collectively influence the magnetization process within the same layered crystallographic framework.

Cu-PEA exhibits clear ferromagnetic hysteresis loops between 2 and 15 K in both in-plane and out-of-plane configurations. The maximum magnetization values at 7T are approximately 6189 emu·mol^{-1} (in-plane) and 5496 emu·mol^{-1} (out-of-plane) at 2 K. The slightly higher saturation magnetization in the in-plane direction indicates anisotropic spin alignment within the layered structure, consistent with the two-dimensional nature of the Ruddlesden–Popper framework. In contrast, Mn-PEA displays predominantly antiferromagnetic characteristics. The M–H curves show nearly linear field dependence without clear saturation, particularly in the out-of-plane direction. In the out-of-plane configuration, a field-induced anomaly is observed between 2 and 30 K, consistent with a spin-reorientation or spin-flop–like transition commonly associated with antiferromagnetic systems. These features highlight the strong directional dependence of magnetic interactions in Mn-PEA, reflecting anisotropic exchange coupling within the layered crystal structure.

The Cu_xMn_{1-x}-PEA samples exhibit composition-dependent field-dependent magnetization behavior. At 2 K, all mixed compositions display hysteresis loops in both in-plane and out-of-plane configurations, indicating the presence of ferromagnetic exchange contributions inherited from the Cu-

Sample	T_C/T_N (K)	ϑ_{CW} (K)	*g*-factor	*J* (meV)	*C* (emu·K·mol^{-1})	μ_{eff} (μ_B)
Cu-PEA	T_C=12±1	17.4±0.5	2.05±0.05	2.21±0.05	0.397	1.78
$Cu_{0.75}Mn_{0.25}$-PEA	T_C=12±1	16.2±0.5	2.68±0.05	0.680±0.005	0.980	2.80
$Cu_{0.50}Mn_{0.50}$-PEA	T_C=12±1	13.9±0.5	3.17±0.05	0.279±0.005	1.76	3.75
$Cu_{0.25}Mn_{0.75}$-PEA	T_C=12±1	14.8±0.5	1.87±0.05	0.394±0.005	1.16	3.05
Mn-PEA	T_N=44±0.5	-117±2	2.02±0.05	0.79±0.03	3.20	5.06

Table1. Summary of magnetic parameters extracted from Curie-Weiss and two-dimensional Heisenberg model fitting for Cu_xMn_{1-x}-PEA single crystal.

View Article Online
DOI: 10.1039/D6TC00615A

containing framework. However, the saturation magnetization decreases progressively with increasing Mn content, reflecting the growing influence of antiferromagnetic Mn-centered interactions. The $Cu_{0.50}Mn_{0.50}$-PEA sample shows a magnetization magnitude comparable to that of Cu-PEA at low fields, suggesting a non-linear evolution of magnetic response with composition. Rather than indicating enhanced ferromagnetic coupling, this behavior likely arises from competing exchange interactions and compositional modulation within the same layered crystallographic framework. Overall, the systematic variation of hysteresis shape, saturation magnetization, and anisotropy with Mn concentration demonstrates that the magnetic properties of the Cu_xMn_{1-x}-PEA system are governed by the interplay between Cu-related ferromagnetic exchange and Mn-related antiferromagnetic interactions, rather than by a simple additive superposition of the two end-member phases.

Experimental

Materials and Syntheses

Phenylethylamine (PEA, $C_6H_5CH_2CH_2NH_2$), copper(II) chloride dihydrate ($CuCl_2{\cdot}2H_2O$, ≥ 99.0%), manganese(II) chloride tetrahydrate ($MnCl_2{\cdot}4H_2O$, ≥ 98%), hydrochloric acid (HCl, 35 wt% in water), methanol (MeOH, ≥ 99.8%), and acetonitrile (AN, ≥99.5%) were purchased from Duksan. All chemicals were used as received without further purification.

PEA·HCl was prepared by adding concentrated hydrochloric acid (~ 2 equiv.) dropwise to phenylethylamine under stirring at room temperature. The resulting solution was evaporated to dryness to afford a slightly yellowish solid, which was dried under ambient conditions for 12 h. The solid was then washed with diethyl ether by filtration and dried at room temperature for 24 h, yielding a white powder composed of plate-like crystalline flakes.

For the synthesis of Cu-PEA and Mn-PEA single crystals, PEA·HCl (0.021 mol, 3.31 g) was dissolved in methanol (50 mL) (colorless solution). $CuCl_2{\cdot}2H_2O$ (0.01 mol, 1.54 g) and $MnCl_2{\cdot}4H_2O$ (0.01 mol, 1.98 g) were each separately dissolved in methanol (50 mL)(transparent yellow-orange solution for the Cu-containing precursor and highly transparent pale pink solution for the Mn-containing precursor). The corresponding metal chloride solutions were then combined with the PEA·HCl solution to form a clear precursor solution. A slight excess of PEA·HCl was employed to ensure complete coordination with the metal ions and to facilitate crystal formation.

For the synthesis of mixed compositions Cu_xMn_{1-x}-PEA (x = 0.75, 0.50, 0.25), the samples were prepared using the same procedure as described above, with only the molar ratio $CuCl_2{\cdot}2H_2O$ to $MnCl_2 \cdot 4H_2O$ adjusted to achieve the desired compositions.

The five precursor solutions prepared as described above were each transferred to a 200 mL beaker and carefully layered with acetonitrile (50 mL) to induce slow diffusion. The beakers were sealed with parafilm, in which approximately 10 small holes were made, and kept at 40 °C to allow slow solvent evaporation. Single crystals suitable for analysis were obtained after approximately two weeks. The crystals were collected by filtration, washed with cold methanol, and dried under ambient conditions.

Structural and Magnetic Characterization

Powder X-ray diffraction measurements were carried out using a Rigaku MiniFlex600 diffractometer with Cu Kα radiation at room temperature. The diffraction data were indexed to determine lattice parameters and space group symmetry. In addition, powder X-ray diffraction (PXRD) data for the Cu-PEA and Mn-PEA samples were refined using the Rietveld method implemented in the FullProf suite. The refinements showed reasonable agreement between the observed and calculated patterns, allowing reliable determination of peak positions and extraction of structural parameters. Based on these analyses, Cu-PEA and Mn-PEA were confirmed to adopt the same layerd framework (Pbca). Magnetic properties were measured using a vibrating sample magnetometer (VSM) integrated within a Physical Property Measurement System (PPMS, Quantum Design). Temperature-dependent magnetization (M–T) measurements were carried out between 2 and 300 K under an applied magnetic field of 1000 Oe. Field-dependent magnetization (M–H) curves were recorded in magnetic fields up to ±7 T.

Conclusions

In summary, we have investigated the composition-dependent magnetic properties of two-dimensional Ruddlesden-Popper hybrid perovskite single crystals, Cu_xMn_{1-x}-PEA (x-0, 0.25, 0.50, 0.75, 1). All compositions adopt a common orthorhombic layered framework, within which compositional mixing dreves a continuous evolution of magnetization magnitude and magnetic anisotorpy. Cu-PEA exhibits ferromagnetic ordering at T_C = 12 K, while Mn-PEA displays antiferromagnetic behaviore with T_N = 44 K. The mixed compositions display composition-dependent magnetic behavior governed by the interplay of Cu-centered ferromagnetic and Mn-centered antiferromangetic exchange interactions, as quatified through combined Curie-Weiss and two-dimensitonal Heisenberg analysis. These results demonstrate that compositional tuning of transition-metal sites provides an effective route to modulating magnetic anisotripy in layered hybrid perovskites, highlighting their potential as tunable low-dimensional magnetic materials. Future work will extend this approach to additional transition-metal systems to further elucidate the relationship between crystal symmetry, exchange interactions, and magnetic anisotropy.

Author contributions

J.K, G.P, K.Y.K, I.O materials synthesis, J.K., D.H, S.K, M.J, H.O, K.S Characterizations. The manuscript was written through contributions of all authors. All authors have given approval to the final version of the manuscript.

Conflicts of interest

There are no conflicts to declare.

Data availability

The data supporting the findings of this study are available within the article and its Electronic Supplementary Information (ESI). Additional data are available from the corresponding author upon reasonable request.

Acknowledgements

This research has received funding support from the National Research Foundation of Korea grants funded by the Government of Korea (RS-2023-00278491 and RS-2023-00280175). This work was supported by Korea Basic Science Institute (National research Facilities and Equipment Center) grant funded by the Ministry of Science and ICT (No. RS-2024-00402995). And this research was supported by the Commercialization Promotion Agency for R&D Outcomes (COMPA) funded by the Ministry of Science and ICT (MSIT)(No. 2710084650).

Notes and references

‡ These authors contributed equally to this work.

1 L. G. Gordeeva, Y. D. Tu, Q. Pan, M. L. Palash, B. B. Saha, Y. I. Aristov, R. Z. Wang, *Nano Energy*, 2021, **84**, 105946.
2 U. Khan, A. Nairan, J. Gao, Q. Zhang, *Small Structures*, 2023, **4**, 2200109.
3 Z.-Z. Ma, Q.-H. Li, Z. Wang, Z.-G. Gu, J. Zhang, *Nat. Commun.*, 2022, **13**, 6347.
4 Y. Peng, S. A. Sanati, Morsali, H. García, *Angew. Chem., Int. Ed.*, 2023, **62**, e202214707.
5 M. Mączka, J. K. Zaręba, A. Gągor, D. Stefańska, M. Ptak, K. Roleder, D. Kajewski, A. Soszyński, K. Fedoruk, A. Sieradzki, *Chem. Mater.,* 2021, **33**, 2331-2342.
6 M.-J. Sun, R. Sabatini, P.-X. Wang, A. M. Najarian, K. Bertens, A. Johnston, S. Hoogland, E. H. Sargent, *Advanced Functional Materials,* 2022, **32**, 2107939.
7 G. Chen, X. Liu, J. An, S. Wang, X. Zhao, Z. Gu, C. Yuan, X. Xu, J. Bao, H.-S. Hu, J. Li, X. Wang, *Nat. Chem.,* 2023, **15**, 1581-1590.
8 H. Zheng, A. Ghosh, M. J. Swamynadhan, Q. Zhang, W. P. D. Wong, Z. Wu, R. Zhang, J. Chen, F. Cimpoesu, S. Ghosh, B. J. Campbell, K. Wang, A. Stroppa, R. Mahendiran, K. P. Loh, *Nat. Commun.,* 2024, **15**, 5556.
9 W. Li, Z. Wang, F. Deschler, S. Gao, R. H. Friend, A. K. Cheetham, *Nat. Rev. Mater.,* 2017, **2**, 16099.
10 Y. Liu, Y. Liu, Y. Guo, *Mater. Chem. Front.,* 2023, **7**, 5215-5246.
11 A. D. Khan, M. Mustajab, S. Moeen, M. Imran, M. Ikram, Q. Khan, M. Khan, *Environ. Sci.: Adv.,* 2024, **3**, 1004-1029.
12 S. Lv, W. Gao, Y. Liu, H. Dong, N. Sun, T. Niu, Y. Xia, Z. Wu, L. Song, C. Ran, L. Fu, Y. Chen, *J. Energy Chem.,* 2022, **65**, 371-404.
13 F. Wang, X. Li, H. Wang, Y. Gou, S. Yang, D. Han, L. Yang, L. Fan, J. Yang, F. Rosei, *Chem. Eng. J.,* 2022, **446**, 137431.
14 D. Li, Y. Huang, Z. Ren, A. Amini, A. B. Djurišić, C. Cheng, G. Li, *J. Energy Chem.,* 2023, **79**, 168-191.
15 J.-P. Correa-Baena, M. Saliba, T. Buonassisi, M. Grätzel, A. Abate, W. Tress, A. Hagfeldt, *Science,* 2017, **358**, 739-744.
16 P. Judeinstein, C. Sanchez, *J. Mat. Chem.,* 1996, **6**, 511-525.
17 B. Saparov, D. B. Mitzi, *Chem. Rev.,* 2016, **116**, 4558-4596.
18 F. Lou, T. Gu, J. Ji, J. Feng, H. Xiang, A. Stroppa, *npj Comput. Mater.,* 2020, **6**, 114.
19 R. Kashikar, P. S. Ghosh, S. Lisenkov, B. R. K. Nanda, I. Ponomareva, *Phys. Rev. B,* 2021, **104**, 235132.
20 H. Mo, Y.-C. Yin, J.-D. Luo, J.-T. Yang, F. Li, D.-M. Huang, H. Zhang, B. Ye, T. Tian, H.-B. Yao, *ACS Appl. Mater. Interfaces,* 2022, **14**, 17479-17485.
21 S. Ullah, A. Andrio, J. Marí-Guaita, H. Ullah, A. Méndez-Blas, R. M. del Castillo Vázquez, B. Mari, V. Compañ, *Phys. Chem. Chem. Phys.,* 2024, **26**, 6736-6751.
22 G. Xing, N. Mathews, S. Sun, S. S. Lim, Y. M. Lam, M. Grätzel, S. Mhaisalkar, T. C. Sum, *Science,* 2013, **342**, 344-347.
23 Q. Lin, A. Armin, R. C. R. Nagiri, P. L. Burn, P. Meredith, *Nat. Photonics,* 2015, **9**, 106-112.
24 A. Marchioro, J. Teuscher, D. Friedrich, M. Kunst, R. van de Krol, T. Moehl, M. Grätzel, J.-E. Moser, *Nat. Photonics,* 2014, **8**, 250-255.
25 L. Protesescu, S. Yakunin, M. I. Bodnarchuk, F. Krieg, R. Caputo, C. H. Hendon, R. X. Yang, A. Walsh, M. V. Kovalenko, *Nano Lett.,* 2015, **15**, 3692-3696.
26 A. Kojima, K. Teshima, Y. Shirai, T. Miyasaka, *J. Am. Chem. Soc.,* 2009, **131**, 6050-6051.
27 J.-W. Lee, N.-G. Park, *Adv. Energy Mater.,* 2020, **10**, 1903249.
28 D. B. Mitzi, *J. Am. Chem. Soc., Dalton Trans.,* 2001, **1**, 1-12.
29 Y. Lu, Q. Wang, L. Han, Y. Zhao, Z. He, W. Song, C. Song, Z. Miao, *Adv. Funct. Mater.,* 2024, **34**, 2314427.
30 K. Liao, X. Hu, Y. Cheng, Z. Yu, Y. Xue, Y. Chen, Q. Gong, *Adv. Opt. Mater.,* 2019, **7**, 1900350.
31 J.-Y. Seo, J. Choi, H.-S. Kim, J. Kim, J.-M. Yang, C. Cuhadar, J. S. Han, S.-J. Kim, D. Lee, H. W. Jang, N. Park, *Nanoscale,* 2017, **9**, 15278-15285.
32 J.-C. Blancon, J. Even, C. C. Stoumpos, M. G. Kanatzidis, A. D. Mohite, *Nat. Nanotechnol.,* 2020, **15**, 969-985.
33 S. Mattioniet,vY. Asensio, P. Solokha, L. Olano-Vegas, M. Prato, S. D. Negri, M. Gobbi, F. Casanova, A. Mateo-Alonso, L. E. Hueso, B. Martín-García, *ACS Appl. Mater. Interfaces*, 2025, **17**, 53745
34 R. Kentsch, *J. Phys. Chem. C,* 2023, **127**, 22222–22233.
35 S. Kassou, *Adv. Com. Hybrid Mater.* 2019**, 2**, 373
36 K.-Y. Kim, G. Park, J. Cho, J. Kim, J.-S. Kim, J. Jung, K. Park, C.-Y. You, I.-H. Oh, *Small,* 2020, **16**, 2005445.
37 A. O. Polyakov, A. H. Arkenbout, J. Baas, G. R. Blake, A. Meetsma, A. Caretta, P. H. M. van Loosdrecht, T. T. M. Palstra, *Chem. Mater.,* 2012, **24**, 133-139.
38 S.-H. Park, I.-H. Oh, S. Park, Y. Park, J. H. Kim, Y.-D. Huh, *Dalton Trans.,* 2012, **41**, 1237-1242.
39 D. B. Losee, W. E. Hatfield, *Phys. Rev. B,* 1974, **10**, 212-218.
40 M. E. Lines, *J. Phys. Chem. Solids,* 1970, **31**, 101-116.